nature microbiology

BRIEF COMMUNICATION

PUBLISHED: 1 AUGUST 2016 | ARTICLE NUMBER: 16124 | DOI: 10.1038/NMICROBIOL.2016.124

Probing the metabolic heterogeneity of live *Euglena gracilis* with stimulated Raman scattering microscopy

Yoshifumi Wakisaka[1†], Yuta Suzuki[2†], Osamu Iwata[3], Ayaka Nakashima[3], Takuro Ito[4,5], Misa Hirose[6], Ryota Domon[6], Mai Sugawara[6], Norimichi Tsumura[6], Hiroshi Watarai[7], Tomoyoshi Shimobaba[8], Kengo Suzuki[3], Keisuke Goda[1,9,10*] and Yasuyuki Ozeki[2*]

Understanding metabolism in live microalgae is crucial for efficient biomaterial engineering, but conventional methods fail to evaluate heterogeneous populations of motile microalgae due to the labelling requirements and limited imaging speeds. Here, we demonstrate label-free video-rate metabolite imaging of live *Euglena gracilis* and statistical analysis of intracellular metabolite distributions under different culture conditions. Our approach provides further insights into understanding microalgal heterogeneity, optimizing culture methods and screening mutant microalgae.

Microalgae-based biomaterials have gained a great deal of attention as food supplements, drugs, biodegradable plastics and biofuels over the past decade[1–3]. Among the various microalgae used for biomaterial production, *Euglena gracilis*, a species of unicellular flagellate protists, is attractive by virtue of its ability to produce both paramylon and lipids[4]. Paramylon is a type of β-1,3-glucan and is a potential drug candidate for several diseases, including HIV infection[5] and colon cancer[6], while lipids can be used as a biofuel alternative to fossil fuels[7]. To produce these biomaterials efficiently, chemically specific analysis of cell-to-cell variations in a heterogeneous population of live *E. gracilis* cells is essential for better understanding their biodiversity, which is more significant under environmental perturbations[8]. The analysis results can then help us develop and optimize the genetic transformation and culture conditions under which the cells alter their metabolism by modifying their biosynthetic pathways towards the formulation and accumulation of the metabolites.

Unfortunately, conventional analytical tools fail to provide such phenotypic specificity. Mass spectrometry and chromatography[9] are incapable of examining cell heterogeneity because they require a large number of cells (~10^5). Coulter counting and fluorescence-activated cell sorting are known as high-throughput methods for counting and analysing a large number of cells[10,11], but they cannot identify morphological attributes and intracellular molecular distributions due to the methods' lack of spatial metrics. Although fluorescence microscopy offers molecular-specific imagery via fluorescent labelling[12], fluorescent dyes can cause cytotoxicity or interfere with cellular metabolism and bioproduct yield[13]. Furthermore, because there are few fluorescent probes for microalgae such as *E. gracilis*, it is not feasible to visualize the various types of intracellular metabolites, including paramylon.

In this Communication, we demonstrate label-free metabolite imaging of live *E. gracilis* at video rate using multicolour stimulated Raman scattering (SRS)—an optical spectroscopic method for probing the vibrational signatures of molecules with orders-of-magnitude higher sensitivity than spontaneous Raman scattering, thereby enabling high-speed Raman image acquisition[14–17]. The key advantage of Raman imaging is its ability to provide submicrometre-resolved intracellular chemical maps for identifying subcellular organelles and biomolecules (for example, paramylon, lipids and chlorophyll in the case of *E. gracilis*) without the need for any exogenous contrast agents such as fluorescent dyes. Coherent anti-Stokes Raman scattering has been applied to the evaluation of microalgae, but its imaging speed is insufficient to analyse motile cells[18,19]. SRS imaging's high frame rate of 110 frames per second (f.p.s.) per spectral point enables us to quantify and analyse previously inaccessible cell-to-cell variations in the metabolite accumulation of a large population of motile *E. gracilis* cells under different culture conditions.

Our SRS microscope is shown schematically in Fig. 1a (see Methods and Supplementary Fig. 1 for details)[16]. This is capable of providing Raman images at 91 spectral points over the entire CH-stretching region (2,800–3,100 cm^{-1}) and a high frame rate of 30 f.p.s. per spectral point with a field of view (FOV) and spatial resolution of 80 × 80 μm^2 and 0.6 μm (horizontal) × 0.6 μm (vertical) × 1.5 μm (axial), respectively, resulting in an acquisition duration of 3 s (Fig. 1b). Through label-free imaging of fixed *E. gracilis*, we first identified four chemical constituents with distinct spectral features (extracted from the points indicated by arrows in Fig. 1c), which allowed us to determine the amount of each constituent in *E. gracilis* by linear decomposition (Supplementary Section 'Image analysis and distribution analysis' and Supplementary Fig. 2). In the decomposed image of *E. gracilis*, two metabolites of interest (that is, paramylon and lipids) are evident, together with two other chemical constituents (that is, chlorophyll and presumably an overlap of protein and nucleic acid, which share similar spectral features), as shown in Fig. 1c.

For blur-free SRS imaging of live *E. gracilis*, which naturally contract and dilate their cell bodies and swim with their flagella,

[1]Department of Chemistry, University of Tokyo, Tokyo 113-0033, Japan. [2]Department of Electrical Engineering and Information Systems, University of Tokyo, Tokyo 113-8656, Japan. [3]Research & Development Department, Euglena Co., Ltd, Tokyo 108-0014, Japan. [4]Institute for Advanced Biosciences, Keio University, Tsuruoka, Yamagata 997-0052, Japan. [5]Graduate School of Media and Governance, Keio University, Fujisawa, Kanagawa 252-8520, Japan. [6]Department of Information Processing and Computer Science, Chiba University, Chiba 263-8522, Japan. [7]Institute of Medical Science, University of Tokyo, Tokyo 108-8639, Japan. [8]Department of Electrical and Electronics Engineering, Chiba University, Chiba 263-8522, Japan. [9]Department of Electrical Engineering, University of California, Los Angeles, California 90095, USA. [10]Japan Science and Technology Agency, Tokyo 102-8666, Japan. †These authors contributed equally to this work. *e-mail: ozeki@ee.t.u-tokyo.ac.jp; goda@chem.s.u-tokyo.ac.jp

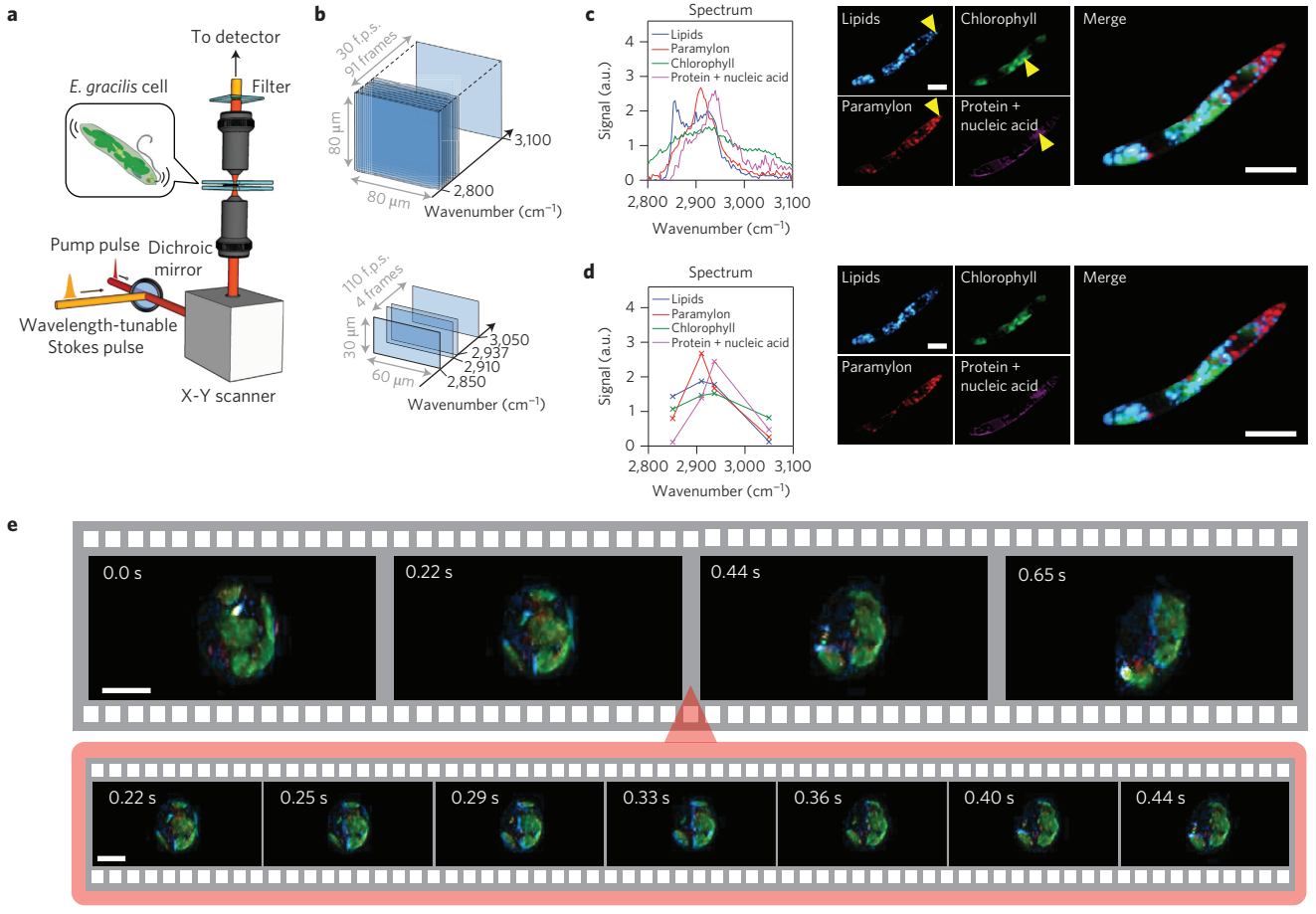

Figure 1 | Label-free video-rate metabolite imaging of *E. gracilis* with a stimulated Raman scattering (SRS) microscope. a, Schematic of the SRS microscope. **b**, Raman image acquisition in different FOVs at 30 and 110 f.p.s. **c**, Imaging of fixed *E. gracilis* at 91 spectral points. The spectra of the chemical constituents were extracted from the points indicated by yellow arrows. **d**, Imaging of fixed *E. gracilis* at four spectral points. **e**, Motion-artefact-free metabolite imaging of a motile *E. gracilis* cell at a video rate of 27 metabolite image frames per second. Scale bars in **c**–**e**, 10 μm. Data shown in **c**–**e** are representative results of more than 20 measurements.

we carefully optimized the imaging parameters for speed improvement without sacrificing image quality and chemical specificity. First, we reduced the number of spectral points to as few as four characteristic colours (2,850, 2,910, 2,937 and 3,050 cm^{-1}) to increase the frame rate by a factor of 91/4 while retaining the chemical specificity of the microscope (Fig. 1d). The frame rate was then increased further by a factor of 3.6 to 110 f.p.s. per spectral point by reducing the FOV to 30×60 μm^2 (although this makes it technically difficult to find and fit the moving cell in the tight FOV). The frame rate of the metabolite imaging was thus boosted by a factor of 83, achieving a video rate of 27 metabolite image frames per second (Fig. 1b). This capability allows for motion-artefact-free and non-invasive metabolite imaging of motile *E. gracilis* cells in as little as 37 ms (Fig. 1e and Supplementary Video 1) and hence image-based monitoring of a large number of individual cells.

Finally, the high-speed multicolour SRS microscope was used to perform population analysis of live *E. gracilis* cells, which were cultured under nitrogen-deficiency stress, a technique for promoting the accumulation of paramylon and lipids within the cell body (see Methods). Specifically, we acquired intracellular metabolite images of three groups of 108 live *E. gracilis* cells (Fig. 2a; for the full library of images see Supplementary Fig. 3) before (day 0) and 2 and 5 days after treatment. Our analysis of the images indicated a gradual change in the cell population's chemical content and hence metabolism (Fig. 2b). The amount of each chemical constituent in each cell was normalized by its cell area (the unnormalized result is shown in Supplementary Fig. 4), although the stress had little effect on cellular size (Fig. 2c). Figure 2d shows projected two-dimensional plots of Fig. 2b, revealing the existence of outliers, which accumulate extraordinary amounts of metabolites (shown in the insets in Fig. 2d). The measurement precision of the SRS microscope was confirmed by the error bars, which represent standard deviations of 24 measured data sets (Fig. 2d). The figure shows the overall tendency for the amounts of both paramylon and lipids to increase over time, while the amount of chlorophyll decreases under the nitrogen-deficient stress, in good agreement with previously reported observations[20]. We conducted statistical analyses on this observed trend, all of which gave significant *P* values (Fig. 2e; see Methods and Supplementary Fig. 5 for details). Thus, our method harnesses heterogeneous cell-to-cell variations in metabolic activity to the macroscopic response of a large number of *E. gracilis* cells.

Here, we have used *E. gracilis* as a model microalgal species and performed metabolite imaging of intracellular paramylon and lipids in each cell, but our method is not limited to this particular species and metabolites. In fact, it is applicable to a diverse range of microalgae, even those with cell walls, such as *Hamakko caudatus*, *Gungnir kasakii* and *Gloeomonas anomalipyrenoides*, as well as other metabolites such as different types of polymers, carotenoids and polysaccharides (for example, starch, amylose and curdlan) (Supplementary Section 'SRS metabolite imaging of other microalgae that contain different polysaccharides' and Supplementary Fig. 6).

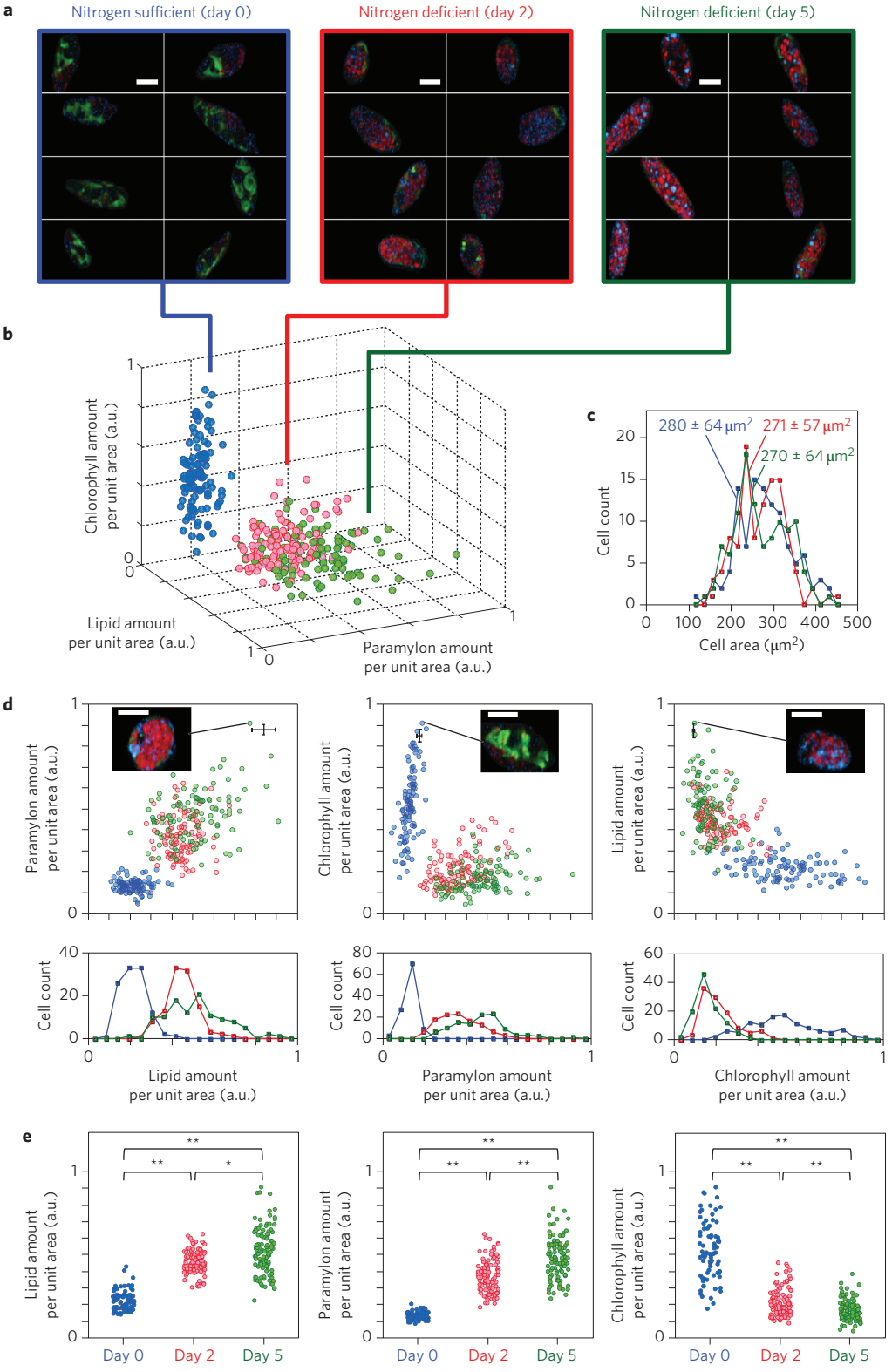

Figure 2 | Statistical analysis of live *E. gracilis* cells under different culture conditions. a, Representative metabolite images of *E. gracilis* cells in the three groups: nitrogen sufficient (day 0) and 2 and 5 days after nitrogen deficiency stress is applied. Colours in the images represent the types of chemical constituents as in Fig. 1d. Scale bars, 10 μm. **b**, Three-dimensional scatter plot of the intracellular amounts of paramylon, lipids and chlorophyll in the three groups of 108 cells. **c**, Histogram of the cell areas of three groups of 108 cells, with their means and standard deviations. **d**, Two-dimensional projections of the three-dimensional scatter plot and histograms of the intracellular amounts. Error bars in the scatter plots represent standard deviations of 24 measurements. Scale bars, 10 μm. **e**, Results of the statistical tests. To conduct the tests, we rejected some data points that had relative standard deviations larger than 0.1 (due to considerable cell movement), resulting in 78, 106 and 108 cells from day 0, 2 and 5 groups, respectively. After verifying significant changes between the groups using the Bartlett and Kruskal–Wallis tests ($P < 0.01$), we conducted the Dunn–Bonferroni test, the results of which are shown as the single ($P < 0.05$) and double ($P < 0.01$) asterisks.

Furthermore, the imaging system allowed us to obtain a three-dimensional metabolite image of live microalgal cells (Supplementary Video 2) for more accurate quantification of the intracellular metabolite content, and we verified strong correlations between the quantified amounts in two and three dimensions (Supplementary Section 'Correlation between 2D and 3D metabolite images' and Supplementary Fig. 8). We anticipate that our method is of prominent importance for further understanding the enormous yet unexplored heterogeneity of microalgae, screening and characterization of microalgal mutants and highly efficient biomaterial engineering.

Methods

SRS microscope. The SRS microscope system was based on two picosecond pulse lasers: a Ti:sapphire pulse laser (Coherent, Mira 900D) and a home-built Yb fibre pulse laser (Supplementary Fig. 1). These lasers were used to generate synchronized pump and Stokes pulse trains with repetition rates of 76 and 38 MHz, respectively. Although the wavelength of the pump laser was 790 nm, that of the Stokes laser was tunable from 1,015 to 1,045 nm. The Stokes laser pulses were equivalent to being intensity-modulated at 38 MHz for lock-in detection. The two laser beams were overlapped both spatially and temporally and were focused onto a target cell via an objective lens (×60, NA 1.2, water). The SRS process occurred within the focused volume of the combined beam inside the target cell, resulting in the transfer of the intensity modulation to the pump beam. The transmitted pump beam was detected by a Si photodetector via another objective lens (×60, NA 1.2, water). The photodetector signal was demodulated by a lock-in amplifier at 38 MHz to obtain the SRS signal. A two-dimensional SRS image was obtained by scanning the combined beam over the target cell with a resonant scanner at 8 kHz and an orthogonally oriented galvanometric scanner, and then digitally mapping the Raman signal into a two-dimensional matrix. During the experiment, artefacts caused by cross-phase modulation parasitic to SRS were found to be negligible (Supplementary Section 'Evaluation of cross phase modulation' and Supplementary Fig. 7). A multicolour image stack was obtained by changing the wavelength of the Stokes laser in a frame by frame manner. The number of pixels in the Raman image was 500 × 500 for the FOV of 80 × 80 μm^2 at 30 f.p.s. per spectral point, and 500 (horizontal) × 116 (vertical) for the FOV of 60 μm (horizontal) × 30 μm (vertical) at 110 f.p.s. per spectral point. For enlarged views, Fig. 1c,d only shows cropped images (50 × 38 μm^2).

Algal material and culture conditions. *Euglena gracilis* NIES-48 was provided by Microbial Culture Collection at the National Institute for Environmental Studies (NIES; http://mcc.nies.go.jp/). The cultures were grown in culture flasks (working volume of 20 ml) under 14:10 light:dark cycle illumination (~140 μmol m^{-2} s^{-1}) at 25 °C. For all the imaging experiments, the stock culture of *E. gracilis* was grown in AF-6 starting with pH 6.6 for at least 6 days as pre-culture. During their exponential growth phase, the cells in AF-6 were regarded as cells in the 'nitrogen-sufficient condition'. The cells in the pre-culture, replaced in AF-6 – N (in which a nitrogen nutrient is omitted from AF-6), were observed to be in the 'nitrogen-deficient condition' after 2 days and 5 days of cultivation. A 10 μl culture solution was placed between coverslips and observed under the SRS microscope. For imaging of fixed *E. gracilis* cells, 0.25% (vol/vol) glutaraldehyde solution was used.

Statistical analysis of intracellular constituents. We examined the statistical significance of the changes in the amount of each cellular constituent (lipids, paramylon and chlorophyll) between the different cell groups using statistical tests. We first calculated the means and standard deviations for each measurement from 24 metabolite images acquired from the same cells. To conduct the tests, we then rejected some data points that had relative standard deviations larger than 0.1, resulting in 78, 106 and 108 cells for the day 0, 2 and 5 groups, respectively. The large relative standard deviations of over 0.1 are presumably due to considerable cell movement during acquisition of the 24 metabolite images, which requires only 0.87 s in total. The means and standard deviations of all the cell images used in the analyses are shown in Supplementary Fig. 5. We first conducted the Bartlett test and found that the variances of the three cell groups are significantly distributed ($P < 0.01$). We therefore performed the non-parametric Kruskal–Wallis test and found that the different cell groups are significantly different ($P < 0.01$) in the amount of each intracellular constituent. After verifying the changes in the amount of each intracellular constituent, we further examined a non-parametric pairwise multiple comparison procedure based on rank sums using the post hoc Dunn–Bonferroni test. As a result, we confirmed significant differences in the change of the amount of each constituent between the different cell groups, with $P < 0.05$ for lipids and $P < 0.01$ for chlorophyll and paramylon, as denoted by the asterisks in Fig. 2e.

Received 15 February 2016; accepted 27 June 2016; published 1 August 2016

References

1. Georgianna, D. R. & Mayfield, S. P. *Nature* **488,** 329–335 (2012).
2. Wijffels, R. H. & Barbosa, M. J. *Science* **329,** 796–799 (2010).
3. Harun, R. *et al. Renew. Sustain. Energy Rev.* **14,** 1037–1047 (2010).
4. Buetow, D. E. *The Biology of Euglena* Vol. 9, Ch. 1 (Academic, 1989).
5. Koizumi, N. *et al. Antiviral Res.* **21,** 1–14 (1993).
6. Watanabe, T. *et al. Food Funct.* **4,** 1685–1690 (2013).
7. Demirbas, A. & Demirbas, M. F. *Energ. Convers. Manage.* **52,** 163–170 (2011).
8. Altschuler, S. J. & Wu, L. F. *Cell* **141,** 559–563 (2010).
9. Lisec, J. *et al. Nature Protoc.* **1,** 387–396 (2006).
10. Graham, M. D. *J. Lab. Autom.* **8,** 72–81 (2003).
11. Bonner, W. A. *et al. Rev. Sci. Instrum.* **43,** 404–409 (1972).
12. Lichtman, J. W. & Conchello, J.-A. *Nature Methods* **2,** 910–919 (2005).
13. Lakowicz, J. R. *Principles of Fluorescence Spectroscopy* (Springer, 2006).
14. Freudiger, C. W. *et al. Science* **322,** 1857–1861 (2008).
15. Cheng, J.-X. & Xie, X. S. *Science* **350,** aaa8870 (2015).
16. Ozeki, Y. *et al. Nature Photon.* **6,** 845–851 (2012).
17. Littlejohn, G. R. *et al. Plant Physiol.* **168,** 18–28 (2015).
18. He, X. N. *et al. Biomed. Opt. Express* **3,** 2896–2906 (2012).
19. Cavonius, L. *et al. Plant Physiol.* **167,** 603–616 (2015).
20. Coleman, L. W. *et al. Plant. Cell Physiol.* **29,** 423–432 (1988).

Acknowledgements

This work was funded mainly by the ImPACT Program of the Council for Science, Technology and Innovation (Cabinet Office, Government of Japan) and partly by Advanced Photon Science Alliance and the Japan Society for the Promotion of Science (JSPS) KAKENHI (grant no. 25702026). Y.S. and K.G. are supported by JSPS and partly by Burroughs Wellcome Fund, respectively.

Author contributions

Y.W. and Y.S. performed the experiments. O.I., A.N. and T.I. prepared the samples. Y.W., Y.S., M.H., R.D., M.S., N.T., T.S. and H.W. performed the data analysis. Y.W., Y.S., K.G. and Y.O. wrote the manuscript. K.G. conceived the concept. K.S., K.G. and Y.O. supervised the work.

Additional information

Supplementary information is available online. Reprints and permissions information is available online at www.nature.com/reprints. Correspondence and requests for materials should be addressed to K.G. and Y.O.

Competing interests

The authors declare no competing financial interests.